DOI: 10.13009/EUCASS2019-371

Nonlinear random response analyses of composite panels under combined supersonic aerodynamic, thermal, and acoustic loads

Hong-Beom Lee[1], Yeong-Nam Kim[2], Jae-Sang Park[3], and In-Gul Kim[4]
Chungnam National University
[1]leehb0721@cnu.ac.kr, [2]kimynrla@cnu.ac.kr, [3]aerotor@cnu.ac.kr, and [4]igkim@cnu.ac.kr

Abstract

This work investigates the nonlinear random vibrations when combined supersonic aerodynamic, thermal, and random acoustic loads are applied to the thin and thick panel structures of high-speed flight vehicles simultaneously. In order to model the thin and thick composite panels, the first-order shear deformation plate theory (FSDT) and the von-Karman nonlinear displacement-strain relationships are applied. The nonlinear equation of motion is derived using the principle of virtual work and the finite element method. Numerical results show the nonlinear dynamic responses such as snapthrough and limit cycle oscillation responses. Particularly, the snapthrough response is caused when the random acoustic load is applied appropriately to the thermally buckled composite plate when the aerodynamic load is not applied or applied with the relatively small magnitude.

1. Introduction

The skin panel structures of supersonic ($1.3 < M < 5.0$) and hypersonic ($5.0 < M < 10$) flight vehicles, such as launch vehicles, guided weapons, and fighter planes, are subjected to combined aerodynamic, thermal, and acoustic loads [1]. The high-speed flight generates significant aerodynamic loads on the skin panel. The thermal loads due to aerodynamic heating cause the thermal buckling and postbuckling of the panel, thus resulting in a sudden change in the vehicle configuration. Additionally, acoustic loads due to engine noise in high-speed flights may induce random vibrations of the panel structures. When the combined aerodynamic, thermal, and random acoustic loads are simultaneously applied to the skin panels, the nonlinear vibration can occur. Nonlinear vibrations were classified [2]: small random vibration on flat position (SV, $w/h < 0.2$), random vibration on buckled position (VBP), snapthrough (ST) response, large random vibration about flat position (LV, $w/h > 2.0$), and limit cycle oscillation (LCO). Among these responses, snapthrough response and limit cycle oscillation have serious influence on the fatigue failure for the high-speed vehicle's skin panel structures [3]. Therefore, it is important to predict the snapthrough response and limit cycle oscillation of the skin panel.

There are various research using numerical methods to analyze the nonlinear dynamic responses for panel structures under combined loads such as thermal and random acoustic loads, or thermal and aerodynamic loads. First, the random vibrations of the plate have been studied under thermal and random acoustic combined loads. The nonlinear random vibration of isotropic panel was investigated using the finite element method [4]. The nonlinear dynamic response was investigated considering thermal, aerodynamic, acoustic loads [4]. In this work, a shape alloy memory(SMA) hybrid panel, as well as isotropic and composite panels were considered. The two studies [2,4] used a thin panel without considering the effects of rotary inertia and transverse shear deformation. The nonlinear random response and fatigue life of the SMA hybrid composite plate [5] and the functionally graded material(FGM) panel [6] were investigated. In these works, the first-order shear deformation plate theory (FSDT) and the von-Karman nonlinear displacement-strain relationships were used for the structural modeling. The nonlinear dynamic behaviors of the thin and thick isotropic panels were analyzed under various thermal and acoustic loading conditions [7]. The panel structure was modeled using the FSDT, and the thermal load was modeled using the assumption that the temperature was uniform along the thickness. The acoustic loads were constructed based on the statistical techniques using a mutual density function. The random dynamic response was investigated when the thermal and acoustic loads were applied to the composite panel [8]. In the study, the differences between the classical plate theory (CPT) and the First-order shear deformation plate theory(FSDT) were compared using the RMS values of the transverse displacements of the composite panels modeled by the two theories.

Second, the nonlinear dynamic responses were investigated under combined thermal and supersonic aerodynamic loads. The finite element equations were formulated to study nonlinear flutter characteristic of the composite plate [9].

DOI: 10.13009/EUCASS2019-371

Various behaviors of the panel under different loading conditions were investigated: Limit cycle oscillation, periodic motion, and chaotic motion. The nonlinear flutter response of stiffened composite laminated plate was investigated [10]. The stiffened plate was modeled using the first-order shear deformation plate theory (FSDT) and Timoshenko beam theory. In addition, the effects of various parameters such as the stiffener, lay-up angle, boundary conditions, and temperature gradient were considered on the panel flutter. The aerothermal postbuckling and nonlinear flutter analyses for the functionally graded materials (FGM) panel were conducted [11]. In the flutter analysis, the stability boundary of the FGM panels was determined with the combined thermal and aerodynamic loads.

Most previous research [2,4,5,9,11] conducted nonlinear dynamic analyses of the panel structures under combined two loads such as thermal and acoustic loads. There have been limited works for nonlinear dynamic analyses when the three loads (aerodynamic, thermal, and acoustic loads) are applied to the composite panel simultaneously. In addition, most of previous studies performed dynamic analyses for the thin panel structures. However, the high-speed flight vehicle's skin structure may be relatively thick because thermal protection system is used. Therefore, it is necessary to consider thick panels as well as thin panels to analyze the nonlinear dynamic behavior of the composite panel structure of high-speed vehicles. This present study investigates the nonlinear dynamic response when combined supersonic aerodynamic, thermal, and random acoustic loads are simultaneously applied to the thin and thick composite panels. The first-order shear deformation plate theory(FSDT) is applied to account for the effects of the rotary inertia and transverse shear deformation. The von-Karman nonlinear displacement-strain relationships are used to express the geometric nonlinearity of the thin and thick composite panels. The nonlinear equation of motion for the composite panel under combined loads are derived using the principle of virtual work and finite element method. The equations of motion are divided into nonlinear static and dynamic equations. The Newton–Raphson method is applied for nonlinear static analysis, and the Newmark-β method is used to examine the nonlinear dynamic behaviors in the time domain. The random acoustic load is modeled using a simple statistical method. The supersonic aerodynamic load is expressed by the first-order piston theory. Using the in-house code with these numerical methods, the nonlinear dynamic responses of both the thin and thick composite panel structures are investigated under various combined aerodynamic, thermal, and acoustic loading conditions. Numerical results show four types of nonlinear dynamic responses: small random vibration, random vibration on buckled position, limit cycle oscillation, snapthrough response for thin and thick composite panels. Among these responses, since the snapthrough and limit cycle oscillation responses have a considerable influence on the fatigue life of the panel, the loading condition to cause the snapthrough and limit cycle oscillation and the displacement response are investigated thoroughly.

2. Formulation

2.1 Nonlinear finite element method

2.1.1 Modeling of thin and thick composite panel structures

The FSDT is used to consider effects of the transverse shear deformation and rotary inertia for thin and thick composite panels. Using the von-Karman displacement-strain relationship to account for geometric nonlinearity, the strain can be written as:

$$\mathbf{e} = \boldsymbol{\varepsilon} - z\boldsymbol{\kappa} = \boldsymbol{\varepsilon}_m + \boldsymbol{\varepsilon}_\theta - z\boldsymbol{\kappa} \tag{1a}$$

$$\boldsymbol{\gamma} = [\gamma_{yz} \quad \gamma_{xz}]^T \tag{1b}$$

$$\boldsymbol{\varepsilon}_m = \left[\frac{\partial u}{\partial x} \quad \frac{\partial v}{\partial y} \quad \frac{\partial u}{\partial y} + \frac{\partial v}{\partial x} \right]^{\mathrm{T}} \tag{1c}$$

$$\boldsymbol{\varepsilon}_\theta = \frac{1}{2}\left[\left(\frac{\partial w}{\partial x}\right)^2 \quad \left(\frac{\partial w}{\partial y}\right)^2 \quad 2\frac{\partial w}{\partial y}\frac{\partial w}{\partial x} \right]^{\mathrm{T}} \tag{1d}$$

$$\boldsymbol{\kappa} = \left[\frac{\partial \psi_x}{\partial x} \quad \frac{\partial \psi_y}{\partial y} \quad \frac{\partial \psi_x}{\partial y} + \frac{\partial \psi_y}{\partial x} \right]^{\mathrm{T}} \tag{1e}$$

$$\boldsymbol{\gamma} = \begin{bmatrix} \dfrac{\partial w}{\partial y} + \psi_y & \dfrac{\partial w}{\partial x} + \psi_x \end{bmatrix}^{\mathrm{T}} \tag{1f}$$

The constitutive equation of the composite panel structure considering temperature in the thickness direction is shown as follows:

$$\begin{Bmatrix} \mathbf{N} \\ \mathbf{M} \end{Bmatrix} = \begin{bmatrix} \mathbf{A} & \mathbf{B} \\ \mathbf{B} & \mathbf{D} \end{bmatrix} \begin{Bmatrix} \boldsymbol{\varepsilon} \\ \boldsymbol{\kappa} \end{Bmatrix} - \begin{Bmatrix} \mathbf{N}_{\Delta T} \\ \mathbf{M}_{\Delta T} \end{Bmatrix} \tag{2a}$$

$$\mathbf{Q} = \mathbf{A}_s \boldsymbol{\gamma} \tag{2b}$$

where the thermal loads are defined by Equation (3) as follows:

$$\begin{Bmatrix} \mathbf{N}_{\Delta T} \\ \mathbf{M}_{\Delta T} \end{Bmatrix} = \int_{-h/2}^{h/2} \bar{\mathbf{Q}} \bar{\boldsymbol{\alpha}} \Delta T \begin{Bmatrix} 1 \\ z \end{Bmatrix} dz \tag{3}$$

In this work, it is assumed that the temperature change, ΔT, is uniform in the thickness direction.

2.1.2 Modal participation factor

The modal participation factor can be used as the criteria to investigate the contribution of a given mode to the dynamic response of a structure. Higher values of modal participation factors indicate stronger contributions to the dynamic response of a structure. On the other hand, modes with low modal participation factors do not affect seriously the response of a structure. The modal participation factor for the general dynamics problem can be calculated as follows [12,13].

$$\mathbf{M}\ddot{\mathbf{d}} + \mathbf{K}\mathbf{d} = \mathbf{F} \tag{4}$$

where **M** is the mass matrix, **K** is the stiffness matrix, $\ddot{\mathbf{d}}$ is the acceleration vector, **d** is the displacement vector, and **F** is excitation force vector.

The homogeneous solution of equation (4) can be obtained in terms of eigenvalues and eigenvectors. The generalized mass matrix ($\hat{\boldsymbol{m}}$) of system is represented by equation (5).

$$\hat{\mathbf{m}} = \boldsymbol{\Phi}^T \mathbf{M} \boldsymbol{\Phi} \tag{5}$$

where $\boldsymbol{\Phi}$ is the eigenvector matrix.

As given in equation (6), the coefficient vector ($\bar{\boldsymbol{L}}$) is derived using the influence vector($\bar{\boldsymbol{r}}$) which represents a rigid body motion.

$$\bar{\mathbf{L}} = \boldsymbol{\Phi}^T \mathbf{M} \bar{\mathbf{r}} \tag{6}$$

The modal participation factors for the i-th mode are calculated as equation (7).

$$\Gamma_i = \frac{\bar{L}_i}{\hat{m}_{ii}} \tag{7}$$

Generally, the lower modes have relatively higher values of modal participation factors. If the value of a modal participation factor of the given mode is reduced suddenly as compared to the values for the previous modes, the modes just prior to this mode can be considered to be important but the modes after this mode are relatively less important to dynamic behaviors of a structure. Thus the cut-off frequency (f_c) in this work is defined using the natural frequency of the mode where its modal participation factor value decreases abruptly. In this present study, the natural frequency of a composite plate in the twentieth mode is selected as the cut-off frequency. In addition, since the time step size (Δt)

DOI: 10.13009/EUCASS2019-371

for the time integration to analyze the dynamic response in time domain is closely related to the cut-off frequency, the time step size can be defined using the equation (8) [14].

$$\Delta t = \frac{1}{2 \times f_c} \tag{8}$$

2.1.3 Modeling of random acoustic load

In order to generate the random acoustic load, a simple statistical method is used in the previous studies [4,6,7]. It is assumed that the random acoustic load acts as a uniformly distributed load on the panel structure and that the mutual spectral density function has a normal Gaussian distribution. The mutual spectral density function is defined using Equation (9), as follows:

$$S_p(f) = \begin{cases} S_0 = p_0^2 10^{SPL/10} & (0 \le f \le f_c) \\ 0 & (f < 0 \quad \text{or} \quad f > f_c) \end{cases} \tag{9}$$

In the present work, the cut-off frequency is determined using the modal participation factors as previously described. Finally, the time varying magnitude random acoustic load, P_{acoustic}, is generated using a random number generation functions, i.e., randn, in MATLAB [2], as follows:

$$P_{\text{acoustic}} = \text{sqrt}(S_0 f_c) \cdot \text{randn}(n,1) \tag{10}$$

where n is the number of time steps for the time integration for a dynamic solution.

2.1.4 Modeling of supersonic aerodynamic load

The supersonic aerodynamic load is modeled based on the first-order piston theory [15, 16] in Equation (11). The first-order piston theory is appropriate to represent the aerodynamic load on the panel in the supersonic region ($\sqrt{2}$<M<5).

$$P_{aero}(x,y,t) = -\frac{\rho_a V_a^2}{\sqrt{M^2-1}} \left\{ \frac{\partial w}{\partial x} + \left(\frac{M^2-2}{M^2-1} \right) \frac{1}{V_a} \frac{\partial w}{\partial t} \right\} = -\left(\lambda \frac{D_{110}}{a^3} \frac{\partial w}{\partial x} + \frac{g_a}{\omega_0} \frac{D_{110}}{a^4} \frac{\partial w}{\partial t} \right) \tag{11}$$

where the nondimensional dynamic pressure, λ, and the nondimensional aerodynamic damping, g_a, are defined as in Equation (12). When the Mach number is relatively high, the aerodynamic damping can be expressed in terms of λ and μ/M which is the air mass ratio with the value or 0.1 or 0.01 [17].

$$\lambda = \frac{\rho_a V_a^2 a^3}{\beta_0 D_{110}} \tag{12a}$$

$$g_a = \frac{\rho_a}{\rho h} \frac{\mu}{\beta_0} \frac{V_a}{\omega_0} \left(\frac{M^2-2}{M^2-1} \right) \simeq \sqrt{\lambda \frac{\mu}{M}} \tag{12b}$$

where D_{110} is the first term of the bending stiffness matrix **D** of a composite panel, when all the fibers are arranged in the direction of the supersonic airflow. In addition, ω_0, β_0, and μ are the convenient reference frequency, the aerodynamic velocity coefficient, and the mass density ratio, respectively. In addition, they are defined as:

$$\omega_0 = \sqrt{\frac{D_{110}}{\rho h a^4}} \tag{13a}$$

$$\beta_0 = \sqrt{M^2 - 1} \tag{13b}$$

$$\mu = \frac{\rho_a a}{\rho h} \tag{13c}$$

2.1.5 Derivation of the equations of motion

Based on the principle of virtual work and finite element method, as presented in Equation (14), the nonlinear equation of motion for the composite panels under combined supersonic aerodynamic, thermal, random acoustic loads are derived as follows:

$$\delta W = \delta W_{\text{int}} - \delta W_{\text{ext}} = 0 \tag{14}$$

The internal work is given

$$\begin{aligned} \delta W_{\text{int}} &= \int_V \delta \mathbf{e}^{\mathrm{T}} \boldsymbol{\sigma} dV \\ &= \int_A \left[\delta \boldsymbol{\varepsilon}^{\mathrm{T}} \mathbf{N} + \delta \boldsymbol{\kappa}^{\mathrm{T}} \mathbf{M} + \delta \boldsymbol{\gamma}^{\mathrm{T}} \mathbf{Q} \right] \\ &= \delta \mathbf{d}^{\mathrm{T}} \left[\mathbf{K}_L - \mathbf{K}_{\Delta T} + \frac{1}{2} \mathbf{K}_{NS1} + \frac{1}{3} \mathbf{K}_{NS2} \right] \mathbf{d} - \delta \mathbf{d}^{\mathrm{T}} \mathbf{F}_{\Delta T} \end{aligned} \tag{15}$$

where the displacement vector is defined as $\mathbf{d}=[\mathbf{u}\ \mathbf{v}\ \boldsymbol{\theta}_x\ \boldsymbol{\theta}_y \mathbf{w}]^{\mathrm{T}}$, $\boldsymbol{K}_{\mathrm{L}}$ and $\boldsymbol{K}_{\Delta \mathrm{T}}$ are the linear stiffness matrix and thermal stiffness matrix, respectively and $\boldsymbol{K}_{\mathrm{NS1}}$ and $\boldsymbol{K}_{\mathrm{NS2}}$ are the first and second order nonlinear stiffness matrices, respectively. On the other hand, the external work is expressed as Equation (16):

$$\begin{aligned} \delta W_{\text{ext}} &= \int_A \delta \mathbf{d}^{\mathrm{T}} (\rho h \ddot{\mathbf{d}} + P_{\text{aero}} - P_{\text{acoustic}}) \\ &= \int_A \begin{bmatrix} -I_0 (\ddot{\mathbf{u}} \delta \mathbf{u} + \ddot{\mathbf{v}} \delta \mathbf{v} + \ddot{\mathbf{w}} \delta \mathbf{w}) + I_1 (\ddot{\mathbf{u}} \delta \boldsymbol{\psi}_x + \ddot{\boldsymbol{\psi}}_x \delta \mathbf{u} + \ddot{\mathbf{v}} \delta \boldsymbol{\psi}_y + \ddot{\boldsymbol{\psi}}_y \delta \mathbf{v}) - I_2 (\ddot{\boldsymbol{\psi}}_x \delta \boldsymbol{\psi}_x + \ddot{\boldsymbol{\psi}}_x \delta \boldsymbol{\psi}_x) \\ -\left(\lambda \frac{\partial \mathbf{w}}{\partial x} + \frac{g_a}{\omega_0} \frac{\partial \mathbf{w}}{\partial t} \right) \delta \mathbf{w} + P_{\text{acoustic}} \delta \mathbf{w} \end{bmatrix} dA \\ &= -\delta \mathbf{d}^{\mathrm{T}} \mathbf{M} \ddot{\mathbf{d}} - \delta \mathbf{d}^{\mathrm{T}} \left(\frac{g_a}{\omega_0} \mathbf{A}_d \dot{\mathbf{d}} + \lambda \mathbf{A}_i \mathbf{d} \right) + \delta \mathbf{d}^{\mathrm{T}} \mathbf{F}_{\text{acoustic}} \end{aligned} \tag{16}$$

When Equations (15) and (16) are inserted into Equation (14), the governing equation for the composite panel under combined supersonic aerodynamic, thermal, and random acoustic loads can be derived as:

$$\mathbf{M} \ddot{\mathbf{d}} + \left(\mathbf{C} + \frac{g_a}{\omega_0} \mathbf{A}_d \right) \dot{\mathbf{d}} + \left(\mathbf{K}_L - \mathbf{K}_{\Delta T} + \lambda \mathbf{A}_i + \frac{1}{2} \mathbf{K}_{NS1} + \frac{1}{3} \mathbf{K}_{NS2} \right) \mathbf{d} = \mathbf{F}_{\Delta T} + \mathbf{F}_{\text{acoustic}} \tag{17}$$

where the structural damping matrix **C** is assumed as proportional damping (Equation 18a), and is added directly to the governing equation. The coefficients α and β for the proportional damping (Equation 18b) are determined using the calculated lowest two natural frequencies (ω_1 and ω_2) and relationship of $\xi_1 \omega_1 = \xi_2 \omega_2$ with $\xi_1 = 0.02$.

$$\mathbf{C} = \alpha \mathbf{M} + \beta \mathbf{K}_L \tag{18a}$$

$$\alpha + \beta \omega_i^2 = 2 \zeta_i \omega_i \tag{18b}$$

The solution of the governing equation can be expressed as the sum of the static and dynamic displacements as:

DOI: 10.13009/EUCASS2019-371

$$\mathbf{d} = \mathbf{d}_s + \mathbf{d}_t \tag{19}$$

By substituting Equation (19) into Equation (17), the static and dynamic equations of motion are written as:

$$\left(\mathbf{K}_L - \mathbf{K}_{\Delta T} + \lambda \mathbf{A}_i + \frac{1}{2}\mathbf{K}_{NS1} + \frac{1}{3}\mathbf{K}_{NS2}\right)\mathbf{d}_s = \mathbf{F}_{\Delta T} \tag{20a}$$

$$\mathbf{M}\ddot{\mathbf{d}}_t + \left(\mathbf{C} + \frac{g_a}{\omega_0}\mathbf{A}_d\right)\dot{\mathbf{d}}_t + \begin{pmatrix}\mathbf{K}_L - \mathbf{K}_{\Delta T} + \lambda \mathbf{A}_i + \mathbf{K}_{NS1} + \mathbf{K}_{NS2} \\ + \mathbf{K}_{ST} + \frac{1}{2}\mathbf{K}_{NT1} + \frac{1}{3}\mathbf{K}_{NT2}\end{pmatrix}\mathbf{d}_t = \mathbf{F}_{\Delta T} + \mathbf{F}_{\text{acoustic}} \tag{20b}$$

2.2 Solution procedure

2.2.1 Solution of nonlinear static equations

The solution of the nonlinear static equation is the postbuckling deflection of the composite panels under combined thermal and supersonic aerodynamic loads. The Newton–Raphson method is applied to solve Equation (20a), and the incremental form at the n-th iteration is expressed as:

$$\left(\mathbf{K}_L - \mathbf{K}_{\Delta T} + \lambda \mathbf{A}_i + \mathbf{K}_{NS1}(\mathbf{d}_s^n) + \mathbf{K}_{NS2}(\mathbf{d}_s^n)\right)\Delta \mathbf{d}_s^{n+1} = \mathbf{P}_{eff}^n \tag{21a}$$

$$\mathbf{P}_{eff}^n = \mathbf{F}_{\Delta T} - \left(\mathbf{K}_L - \mathbf{K}_{\Delta T} + \lambda \mathbf{A}_i + \frac{1}{2}\mathbf{K}_{NS1}(\mathbf{d}_s^n) + \frac{1}{3}\mathbf{K}_{NS2}(\mathbf{d}_s^n)\right)\mathbf{d}_s^n \tag{21b}$$

The nonlinear static displacement is updated as Equation (22):

$$\mathbf{d}_s^{n+1} = \mathbf{d}_s^n + \Delta \mathbf{d}_s^{n+1} \tag{22}$$

where $\mathbf{d}_s^{n+1}$ is the updated static displacement vector and $\Delta \mathbf{d}_s$ is the increment of the static displacement vector. The iterations are continued until the static displacement satisfies the certain convergence tolerance, which is defined as follows:

$$\left\|\mathbf{d}_s^{n+1} - \mathbf{d}_s^n\right\| \le 10^{-5} \tag{23}$$

2.2.2 Solution of nonlinear dynamic equations

The nonlinear dynamic equation is expressed using equation (20b). The Newmark-β time integration method [18] is used to calculate the dynamic displacement($\mathbf{d}_t$). In the time integration, the initial velocity vector ($\dot{\mathbf{d}}_{t0}$) is assumed to be a zero vector but the initial displacement vector ($\mathbf{d}_{t0}$) is assumed appropriately. The acceleration vector ($\ddot{\mathbf{d}}_{t0}$) in Equation (24) is given

$$\ddot{\mathbf{d}}_{t_0} = \mathbf{M}^{-1}\left(\mathbf{F} - \mathbf{K}\mathbf{d}_{t_0} - \mathbf{C}\dot{\mathbf{d}}_{t_0}\right) \tag{24}$$

The dynamic displacement according to the (i+1)th time step is as follows:

$$\Delta \mathbf{d}_t^{i+1} = (\hat{\mathbf{K}}^{i+1})^{-1}\hat{\mathbf{F}}^{i+1} \tag{25}$$

and

$$\hat{\mathbf{K}}^{i+1} = \mathbf{K}^{i+1} + \mathbf{M}^{i+1}\left(a_3\mathbf{d}_t + a_4\dot{\mathbf{d}}_t + a_5\ddot{\mathbf{d}}_t\right) + \mathbf{C}^{i+1}\left(a_6\mathbf{d}_t + a_7\dot{\mathbf{d}}_t + a_8\ddot{\mathbf{d}}_t\right) \tag{26}$$

where the detailed definitions of the coefficients, matrices, and vectors used in Equations (24), (25) and (26) are given in Appendix A.

The updated dynamic displacement is given in Equation (27) and it is calculated iteratively until the convergence tolerance in Equation (28) is satisfied.

$$\mathbf{d}_t^{i+1} = \mathbf{d}_t^i + \Delta\mathbf{d}_t^{i+1} \tag{27}$$

$$\left\|\mathbf{d}_t^{i+1} - \mathbf{d}_t^i\right\| \le 10^{-5} \tag{28}$$

3. Numerical results and discussion

3.1 Validations of numerical analyses codes

Before the nonlinear dynamic responses of composite panels under combined supersonic aerodynamic, thermal, and random acoustic loads are investigated, the numerical analyses codes are validated in order to investigate the accuracy of the finite element formulation in Section 2.

3.1.1 Thermal postbuckling analysis

To verify the postbuckling analysis, the post-buckling deflection is compared with the previous work [19]. The detailed geometric dimensions of a plate, boundary conditions, layup condition, and composite material properties are given in Ref. [19]. As seen in the figure 1, the thermally postbuckled deflection in the present analysis is compared well with the previous analysis [19].

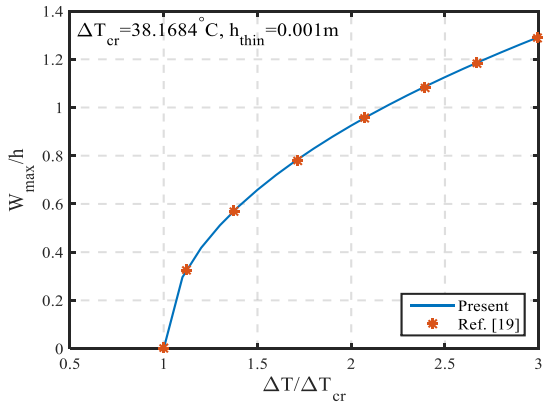

Figure 1. Validation of thermal postbuckling analysis (ΔT_{cr}=38.1684°C).

3.1.2 Nonlinear dynamic analysis

Figure 2 validates the LCO analysis of the thin isotropic plate under the combined supersonic aerodynamic and thermal loads with the previous prediction results [20, 21]. As shown in the Figure, the nondimensionalized amplitudes of LCO in the present work are compared well with the previous analyses [20, 21] at different aerodynamic and thermal loading conditions. Therefore, it is believed that the technique of a dynamic response analysis of a panel structure under combined loads is established well.

DOI: 10.13009/EUCASS2019-371

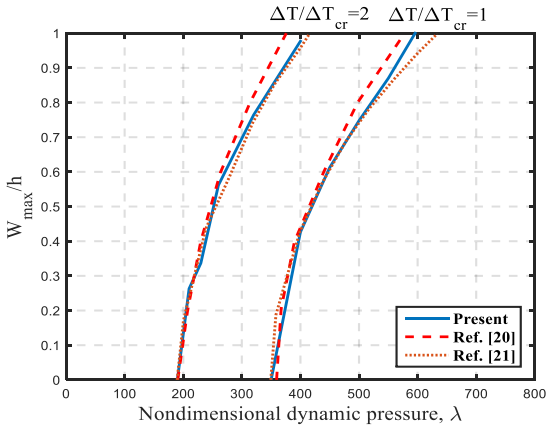

Figure 2. Validation of limit cycle oscillation analysis.

3.1.3 Random acoustic load generation

Table 1 validates the generation of a random acoustic load. For this validation, P_0 and f_c in Equation (4) are assumed to be 20×10^{-6} Pa and 500 Hz, respectively. As shown in the Table 1, the RMS values of the present random loads are compared well with the previous work [2]. In addition, Figure 3 shows an example of time history of the acoustic load for *SPL = 140 dB*.

Table 1. Validation of random acoustic load generation.

	RMS (Pa)		
SPL [dB]	Present	Ref. [2]	Error [%]
110	139.6	142.6	-2.1
120	446.8	448.2	-0.3
130	1414.3	1413.4	-0.007
140	4496.4	4478.8	0.3

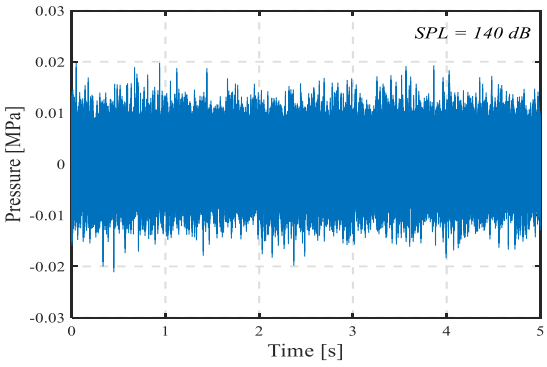

Figure 3. Time history of random acoustic load (*SPL = 140 dB*).

3.2 Finite element modelling

This section shows the results of the numerical analyses using the nonlinear finite element method for simply supported composite plates under combined supersonic aerodynamic, thermal, and random acoustic loads. The plate dimensions are 0.381×0.381×0.0012 m and 0.381×0.381×0.00762 m for the thin and thick plate, respectively. The lay-up condition is $[0/90/45/-45]_S$. The material properties for graphite/epoxy composite material are described in

DOI: 10.13009/EUCASS2019-371

Table 2. The schematic diagram of the composite plate is shown in Figure 4. A uniform 6×6 finite element mesh with nine-node elements is used for the present finite element analysis.

Table 2. Properties of Graphite/Epoxy [9].

Property	Value
E_1	155 GPa
E_2	8.07 GPa
G_{12}	4.55 GPa
ν_1	0.22
α_1	-0.07 × 10^{-6} °C^{-1}
α_2	30.1 × 10^{-6} °C^{-1}
ρ	1550 kg/m^3

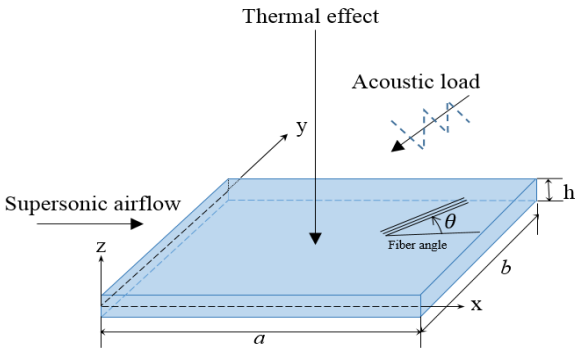

Figure 4. Schematic diagram of a composite plate under combined loads

3.2 Results for thin composite panel

3.2.1 Aerothermal postbuckling analyses

Figure 5 shows the postbuckling analyses of the thin composite panel when the supersonic aerodynamic loads with $\lambda=0$ and 50 are applied to the thin panel. In this example, the critical temperature change of the thin composite panel, $\Delta T_{cr,thin}$ is calculated as $5.9324\ ^{\circ}C$. As shown in Figure 5, the postbuckling deflection is increased nonlinearly as the temperature increases. The maximum nondimensional deflection is calculated at the center of a plate when the thermal load only is considered without the aerodynamic load($\lambda=0$). However, for the aerothermal postbuckling analysis with $\lambda=50$, the nondimensional deflection reduces as compared to the result with $\lambda=0$, because the supersonic aerodynamic load suppresses the postbuckling deflection of the composite plate. As shown in Figure 6, as the nondimensional dynamic pressure (λ) increases from $\lambda=0$ to 90, the position for the maximum deflection is moved toward 75% location in the airflow direction.

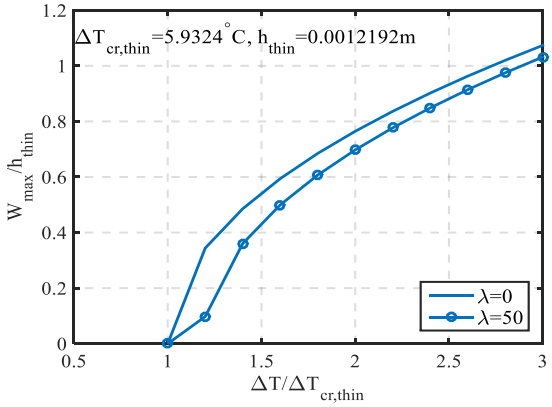

Figure 5. Aerothermal postbuckling analyses (a/h = 312.5).

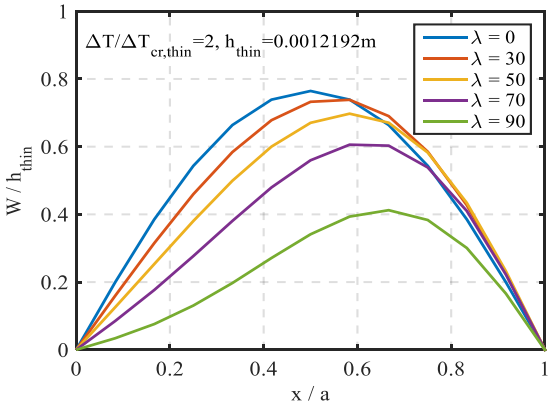

Figure 6. Nondimensional aerothermal postbuckling deflection in x-direction (a/h = 312.5).

3.2.2 Nonlinear dynamic analyses

In this section, the nonlinear dynamic behaviors of a thin composite panel are studied when three loads (supersonic aerodynamic, thermal, and random acoustic loads) are applied to the thin composite plate simultaneously. Figure 7 shows the nonlinear dynamic responses when the thermal and supersonic aerodynamic loads are considered ($\Delta T/\Delta T_{cr,thin} = 2$ and $\lambda=350$) simultaneously. Figure 7 shows the LCO motion with a constant amplitude, because of the geometric nonlinearity of the panel structure [9]. This behavior can affect the fatigue life of the panel of a high-speed flight vehicle because the fatigue is accumulated during the oscillation of a panel with a constant amplitude.

DOI: 10.13009/EUCASS2019-371

Figure 8 shows the nonlinear random vibration for thin composite panel when the random acoustic load is applied without thermal and aerodynamic loads. The small random vibration (SV, w/h < 0.2) is observed at this loading condition (ΔT=0, λ=0, and *SPL=80 dB*). Figures 9 and 10 show the nonlinear random vibration for thin composite panel under combined thermal and random acoustic loads. As shown in Figure 9, the random vibration for buckled position is observed when the combined loads ($\Delta T/\Delta T_{cr,thin}$=2 and *SPL=80 dB)* are considered. Figure 10 presents the ST response at $\Delta T/\Delta T_{cr,thin}$=2 and *SPL=95 dB*. The ST response is the unique random dynamic response which is observed when the random acoustic load with the appropriate magnitude is applied to the thermally postbuckled plate. As shown in Figure 10, The panel shows random vibration at the positive and negative deflected positions alternately. Although the stress response for the ST is not included in this paper, the ST response may have a serious effect on the fatigue life of the composite panel because of the sudden changes of the stress sign. As shown in Figures 8 to 10, the different loading conditions of the combined thermal and acoustic loads result in different nonlinear dynamic responses of the thin composite panel. In addition, it can be seen that the maximum displacement occurs at the center of the plate when the aerodynamic load is not applied.

Figure 11 represents the nonlinear random response of the thin composite panel when three loads (supersonic aerodynamic, thermal, and random acoustic loads) are applied to the thin plate simultaneously. The thermal and acoustic loads to cause the ST response ($\Delta T/\Delta T_{cr,thin}$=2 and *SPL=95 dB*) in Figure 10 are used and the supersonic aerodynamic loads with (λ=*50* and *95*) are applied additionally to the composite plate in this example. Figure 11(a) still exhibits the snapthrough response even though the supersonic aerodynamic load with λ=*50* is additionally applied to the composite panels. However, when the magnitude of the aerodynamic load increases to λ=*95*, as seen in Figure 11(b), the ST response is not shown; instead the nonlinear random vibration is observed. This is because the supersonic aerodynamic load with an appropriate magnitude weakens the effect of the random acoustic load which causes the ST response. In addition, the location of the maximum deflection of the plate is moved from the center of a plate to the near 75% position in the airflow direction, as the supersonic aerodynamic load increases, although this result is not shown herein. As seen in Figures 8 to 11, the nonlinear dynamic responses of a thin composite plate are not as intuitive as the result in LCO in Figure 7 because of the unique characteristics of random vibration.

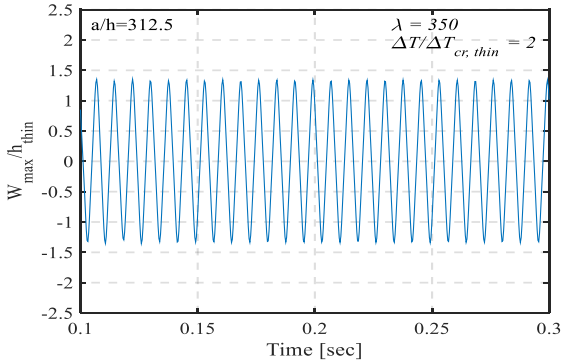

Figure 7. Limit cycle oscillation response (a/h = 312.5).

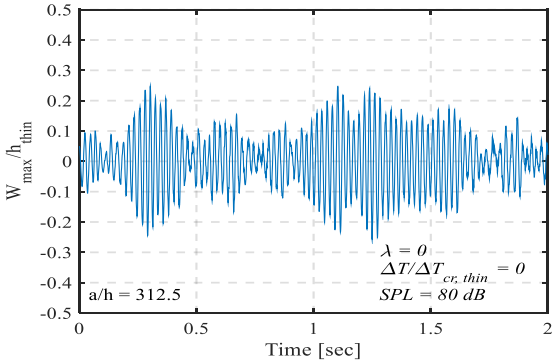

Figure 8. Small random vibration about flat position (a/h = 312.5).

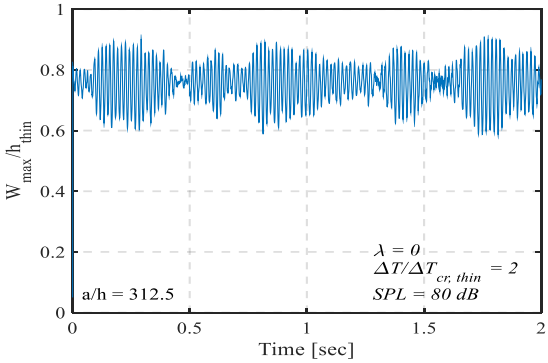

Figure 9. Random vibration on buckled position (a/h = 312.5).

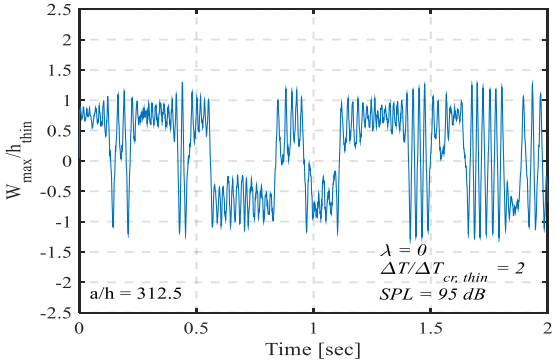

Figure 10. Snapthrough response (a/h = 312.5).

DOI: 10.13009/EUCASS2019-371

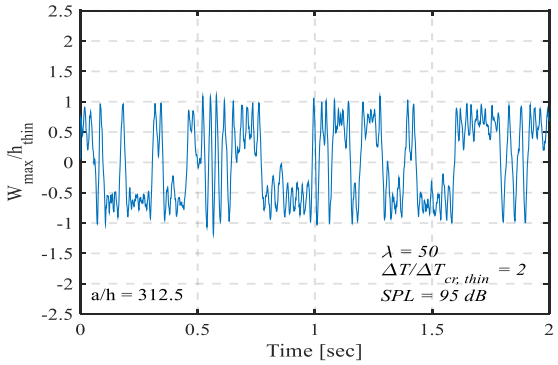

Figure 11(a). Snapthrough response for combined supersonic aerodynamic, thermal, and random acoustic loads (a/h = 312.5).

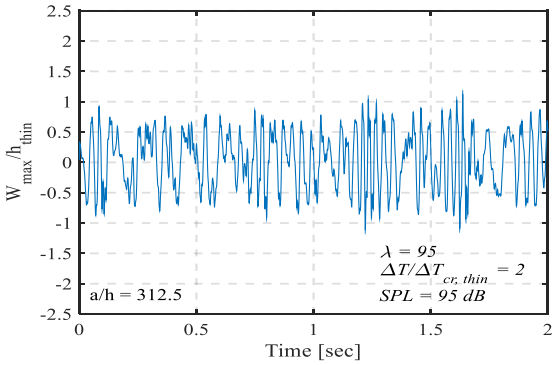

Figure 11(b). Random response for combined supersonic aerodynamic, thermal, and random acoustic loads (a/h = 312.5).

3.3 Results for thick composite panel

3.3.1 Aerothermal postbuckling analyses

The postbuckling analysis of the thick composite panel under combined thermal and supersonic aerodynamic loads (λ=0 and 50) is conducted in Figure 12. In addition, the critical temperature change of the thick composite panel, $\Delta T_{cr,thick}$ is calculated as 229.3424 $^{\circ}C$. Comparing the critical temperature change of the thin composite plate in the previous section, the critical temperature change of the thick plate is higher by approximately 40 times that of the thin composite panel. In the figure, as the temperature increases, the nondimensional maximum deflection of the thick composite panel increases monotonically. Similar to the previous result for the thin composite panel, when the supersonic aerodynamic load is applied to the thick composite panel, it suppresses the thermally buckled panel, thus the maximum deflection reduces. In addition, the position for the maximum deflection is moved toward the 75% location in the airflow direction as the nondimensional dynamic pressure increases, as shown in Figure 13.

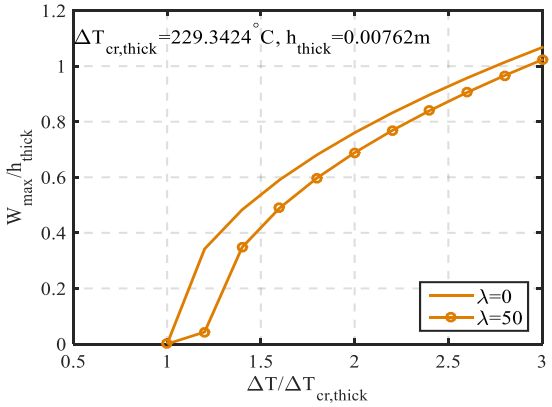

Figure 12. Aerothermal postbuckling analyses (a/h = 50).

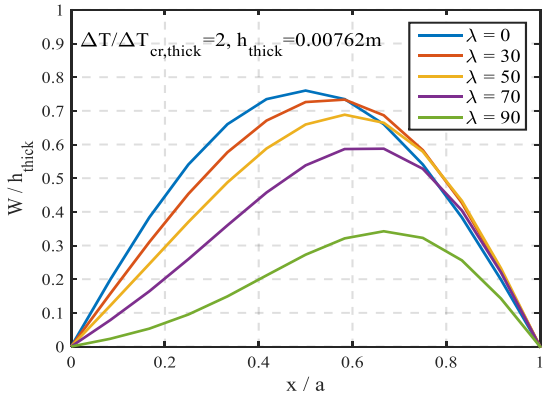

Figure 13. Nondimensional aerothermal postbuckling deflection in x-direction (a/h = 50).

3.3.2 Nonlinear dynamic analyses

In this section, the nonlinear dynamic behaviors of the thick composite panel under combined supersonic aerodynamic, thermal, and random acoustic loads are investigated. Figure 14 shows the nonlinear dynamic response when the thermal and supersonic aerodynamic loads are applied ($\Delta T/\Delta T_{cr,thick}$=2 and λ=300). Figure 14(a) shows the LCO motion with a constant amplitude.

Figure 15 shows the random responses of the thick composite plate when only the random acoustic load is applied ($\Delta T/\Delta T_{cr,thick}$=0, λ=0, and SPL=130 dB). At this loading condition, the thick composite panel exhibits the SV response (w/h < 0.2) at a flat position.

DOI: 10.13009/EUCASS2019-371

The VBP response in Figure 16 shows that the plate is thermally buckled in the upward (positive) direction and a weak nonlinear vibration exists ($\Delta T/\Delta T_{cr,thick}$=2 and *SPL = 130 dB*). Figure 17 exhibits the ST response of the thick composite panel when the thermal load is $\Delta T/\Delta T_{cr,thick}$=2 and the magnitude of the random acoustic load is increased to *SPL=150 dB*. The ST response in the figure shows random vibrations alternatively at the upward and downward deflected positions

Figure 18 shows the nonlinear random vibration of the thick composite plate under the combined supersonic aerodynamic, thermal, and random acoustic loads. In Figure 18, the different supersonic aerodynamic loads with λ*=50* and *100* are additionally considered to the thermal and acoustic loads ($\Delta T/\Delta T_{cr,thick}$=2 and *SPL = 150 dB*) which cause the ST response shown in Figure 17 previously. As shown in the figure 18(a), when the magnitude of the supersonic aerodynamic load is relatively low (λ*=50*), the ST response is still observed. However, when the supersonic aerodynamic load increases to λ*=100*, the ST response is not shown in Figures 18(b); instead, the nonlinear random dynamic response is observed.

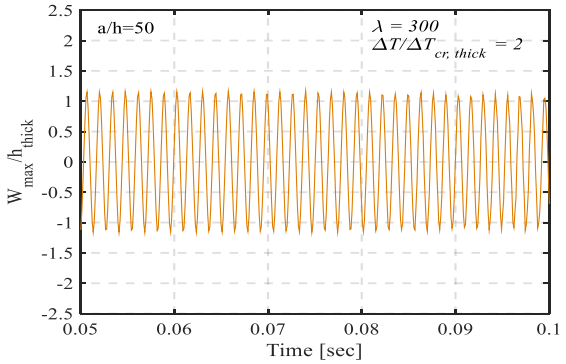

Figure 14. Limit cycle oscillation response (a/h = 50).

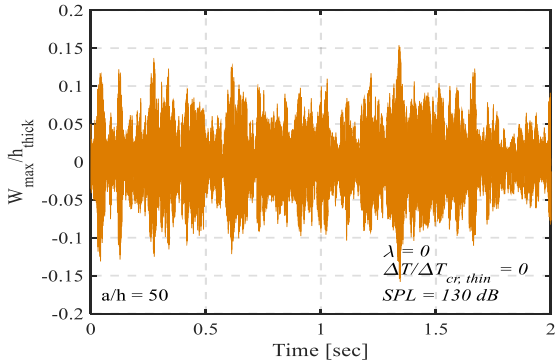

Figure 15. Small random vibration about flat position (a/h = 50).

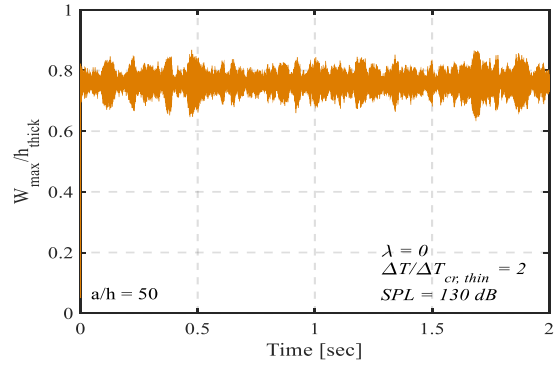

Figure 16. Random vibration on buckled position (a/h = 50).

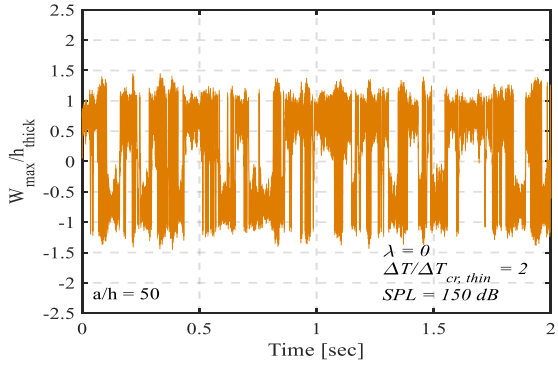

Figure 17. Snapthrough response (a/h = 50).

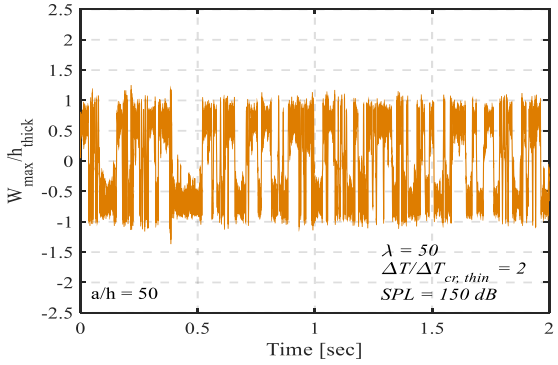

Figure 18(a). Snapthrough response for combined supersonic aerodynamic, thermal, and random acoustic loads (a/h = 50).

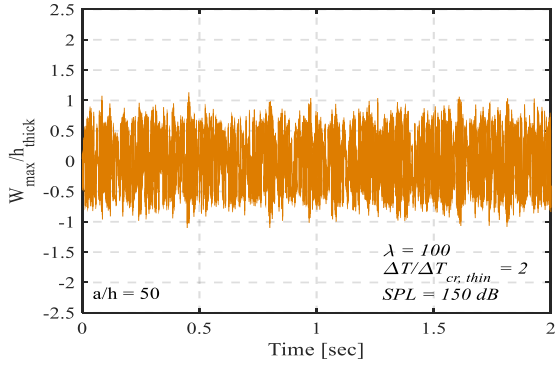

Figure 18(b). Random response for combined supersonic aerodynamic, thermal, and random acoustic loads (a/h = 50).

4. Conclusion

This study conducted the nonlinear dynamic analyses of thin and thick composite panels under combined supersonic, thermal, and random acoustic loads. The panel structures were modeled based on the FSDT, in order to consider the effects of the transverse shear deformation. The von-Karman nonlinear displacement-strain relationship was used to consider the geometric nonlinearity of transverse large deflection of the panels. The supersonic aerodynamic load was modeled using the first-order piston theory. The temperature change(ΔT) was assumed to be constant in the thickness direction. The random acoustic load was represented as stationary white-Gaussian random pressure with zero mean and uniform magnitude over the panels. The nonlinear equation of motion of the composite panels under combined loads was derived using principle of virtual work and finite element method. The governing equation was divided into the nonlinear static and dynamic equations. The Newton–Raphson method was used for the aerothermal postbuckling analysis. The nonlinear dynamic equation in the time domain was solved using the Newmark-β time integration method. The nonlinear dynamic responses under the combined thermal, acoustic, and aerodynamic loads were examined in the time domain. For the thin composite panel, the ST response was exhibited at $\Delta T/\Delta T_{cr,thin}$=2 and *SPL = 95 dB* and LCO motion was investigated at $\Delta T/\Delta T_{cr,thin}$=2 and λ=*350*. On the other hand, for the thick composite panel, the ST response was observed at $\Delta T/\Delta T_{cr,thick}$=2 and *SPL = 150 dB* and the LCO motion caused at $\Delta T/\Delta T_{cr,thick}$=2 and λ=*300*. In addition, for the thin composite panel, the ST response disappears as λ increases from 50 to 95, and the ST behavior vanished as λ increases to 100 for the thick composite panel.

Appendix A

The coefficients, matrices, and vectors for the Newmark-β time integration are defined as follows

$$a_1=\alpha\Delta t,\quad a_2=(1-\alpha)\Delta t,\quad a_3=\frac{1}{\beta(\Delta t)^2},\quad a_4=a_3\Delta t$$
$$a_5=\frac{1}{\gamma}-1,\quad a_6=\frac{\alpha}{\beta\Delta t},\quad a_7=\frac{\alpha}{\beta}-1,\quad a_8=\left(\frac{\alpha}{\gamma}-1\right)\Delta t \tag{A.1}$$
$$\alpha=\frac{1}{2},\quad \beta=\frac{1}{4},\quad \gamma=2\beta$$

$$\hat{\mathbf{F}}^{i+1}=\mathbf{F}_{eff}^{i+1}+\mathbf{M}^{i+1}(a_3\mathbf{d}_t^i+a_4\dot{\mathbf{d}}_t^i+a_5\ddot{\mathbf{d}}_t^i) \tag{A.2}$$

$$\mathbf{F}_{eff}^{i+1}=\mathbf{F}^{i+1}+\mathbf{M}^{i+1}\left(a_3\mathbf{d}_t+a_4\dot{\mathbf{d}}_t+a_5\ddot{\mathbf{d}}_t\right)+\mathbf{C}^{i+1}\left(a_6\mathbf{d}_t+a_7\dot{\mathbf{d}}_t+a_8\ddot{\mathbf{d}}_t\right) \tag{A.3}$$

$$\ddot{\mathbf{d}}_t^{i+1}=a_3\left(\mathbf{d}_t^{i+1}-\mathbf{w}_t^i\right)-a_4\dot{\mathbf{d}}_t^i-a_5\ddot{\mathbf{d}}_t^i \tag{A.4}$$

$$\dot{\mathbf{d}}_t^{i+1}=\dot{\mathbf{d}}_t^i+a_2\ddot{\mathbf{d}}_t^i+a_1\ddot{\mathbf{d}}_t^{i+1} \tag{A.5}$$

Acknowledgment

This study was supported by the Agency for Defense Development. (Assignment number: ADD-06-201-801-014)

References

[1] Oden, J. T., and Thornton, E. A. 1988. Analysis of flow-, thermal-and structural-interaction of hypersonic structures subjected to severe aerodynamic heating. *AirForce Office of Scientific Research*, TR-88-12.

[2] Duan, B. 2001. Suppression of composite panel vibration under combined aerodynamic and acoustic excitations at elevated temperatures using shape memory alloy. Ph.D Thesis. Old Dominion University.

[3] Dowell, E. H. 1996. Nonlinear oscillations of a fluttering plate. *AIAA journal*. 4(7): 1267-1275.

[4] Dhainaut, J. M., Guo, X., and Mei, C., Spottswood, S. M., and Wolfe, H.G. 2003. Nonlinear random response of panels in an elevated thermal-acoustic environment. *Journal of aircraft* 40(4): 683-691.

DOI: 10.13009/EUCASS2019-371

[5] Ibrahim, H. H., Tawfik, M., and Negm, H. M. 2008. Thermoacoustic random response of shape memory alloy hybrid composite plates. *Journal of aircraft* 45(3): 962-970.

[6] Ibrahim, H. H., Yoo, H. H., Tawfik, M., and Lee, K. S. 2010. Thermo-acoustic random response of temperature-dependent functionally graded material panels. *Computational Mechanics* 46(3): 377-386.

[7] Kim, Y. N, Park, J. –S., Jeon, M. H., Go, E. S., and Kim, I.G. 2018. Nonlinear random response analyses of panels considering transverse shear deformations under combined thermal and acoustic loads. *Shock and Vibration.*

[8] Lu, Y. 2008. Random vibration analysis of higher-order nonlinear beams and composite plates with applications of ARMA models. Ph.D Thesis. Virginia Polytechnic Institute and State University.

[9] Zhou, R. C., Xue, D. Y., and Mei, C. 1994. Finite element time domain-modal formulation for nonlinear flutter of composite panels. *AIAA journal* 32(10): 2044-2052.

[10] Lee, I., Lee, D. M., and Oh, I. K. 1999. Supersonic flutter analysis of stiffened laminated plates subject to thermal load. *Journal of Sound and Vibration* 224(1): 49-67.

[11] Sohn, K. J., and Kim, J. H. 2009. Nonlinear thermal flutter of functionally graded panels under a supersonic flow. *Composite Structures* 88(3): 380-387.

[12] Irvine, T. 2013. Effective modal mass & modal participation factors. *Available on the web on site: http://www. vibrationdata.com/tutorials2/ModalMass. pdf (accessed 12 June. 2019).*

[13] Case, J. J. 2017. Numerical analysis of the vibration and acoustic characteristics of large power transformers. Master Thesis. Queensland University of Technology.

[14] Hardin, J. C. 1986. Introduction to time series analysis. NASA-RP-1145.

[15] Ashley, H. 1956. Piston theory-a new aerodynamic tool for the aeroelastician. *Journal of the Aeronautical Sciences* 23(12): 1109-1118.

[16] Dowell, E. H. 1970. Panel flutter-A review of the aeroelastic stability of plates and shells. *AIAA journal* 8(3): 385-399.

[17] Pidaparti, R. M. V., and Yang, H. T. Y. 1993. Supersonic flutter analysis of composite plates and shells. *AIAA journal* 31(6): 1109-1117.

[18] Reddy, J. N. 2006. *An introduction to the finite element method*, 3rd edn. McGraw-Hill, New York, pp 324-326.

[19] Averill, R., and Reddy, J. N. 1993. Thermomechanical postbuckling analysis of laminated composite shells. *34th Structures, Structural Dynamics and Materials Conference.*

[20] Dowell, E.H. 1996. Nonlinear oscillations of a fluttering plate. *AIAA journal* 4(7): 1267-1275.

[21] Xue, D.Y., and Mei, C. 1993. Finite element nonlinear panel flutter with arbitrary temperatures in supersonic flow. *AIAA journal* 31(1): 154-162.